



Polarization-Maintaining Diffractive Elements for Off-Axis Terahertz Digital Holography

Artur Sobczyk¹ · Michał Makowski¹ · Adam Kowalczyk¹ · Jarosław Suszek¹ · Maciej Traczyk¹ · Maciej Sypek¹

Received: 13 October 2022 / Accepted: 17 March 2023 / Published online: 23 March 2023
© The Author(s) 2023

Abstract

Off-axis digital holography in the terahertz waves allows three-dimensional visualizations of optically opaque volumetric objects in a single exposure and with angular separation of the zero-order component. Forming the tilted reference beam usually requires a set of mirrors, which can disturb the polarization, causing the loss of contrast in fringes at the detector. Here we present a mirror-less approach with 3D-printed transmissive diffractive optical elements, providing unaltered polarization and successful holographic measurements at 0.1 THz without any pre- or post-processing of interference fringes.

Keywords Terahertz · Digital holography · Diffractive optical elements

In most cases off-axis interferometric optical setups used for digital holography [1, 2] use flat mirrors [3] to split and guide the beams to the distal [4] detection plane. In the case of terahertz radiation, the sources typically emit highly divergent beams, which additionally need to be collimated with expensive parabolic off-axis mirrors [5], that also induce geometrical aberrations [6, 7], which increase the errors in phase measurements [8]. With wavelengths in the range of millimeters, the apertures and volumes of the involved elements quickly grow to problematic values [9]. Moreover, such bulky reflective elements tend to disturb the state of polarization of the THz beams, affecting the contrast of interference patterns [10]. In this work we present the design and experimental use of 3D-printed transmissive diffractive optical elements [11] (DOE) allowing polarization-maintained, high-contrast interference in off-axis THz digital holography.

The experimental setup is depicted in Fig. 1. The 180-mW TeraSense source at 96.9 GHz (a) emits the divergent coherent THz beam via a 26-dB detachable horn antenna (b). The source uses a standard IMPATT diode. The divergent beam is

✉ Michał Makowski
michal.makowski@pw.edu.pl

¹ Faculty of Physics, Warsaw University of Technology, PL00662, Warsaw, Poland

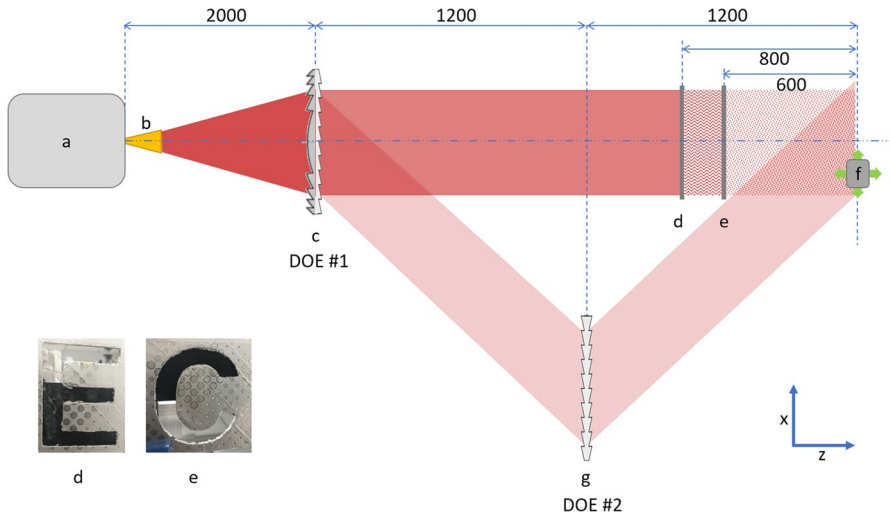


Fig. 1 Scheme of the experimental setup with real distances shown in millimeters. Angles and distances are not to scale for clarity

collimated by the first side of the DOE#1 (c) with diffractive grooves representing the phase delay of a $f = 2000$ mm spherical lens. The relief depth was experimentally optimized to introduce $0-2\pi$ phase shifts at 0.1 THz, so as to ensure the maximal collimation efficiency with minimal zero-order light passing through the structure. The other side of DOE#1 (c) is a sawtooth diffractive grating with deliberately lowered modulation depth, so as to split the collimated beam into the object beam (ca. 80% of power) and into the off-axis reference beam (ca. 20% of power). Again, the depth of the relief was experimentally optimized so as to achieve this assumed division of power. Specifically, a series of gratings was printed with variable relief depths in 1% increments of the numerically obtained value. Then the optimal element was selected after direct and separate measurements of THz power of object and reference beams by averaging the non-saturated readouts from 100 central positions of the detector. The period of the grating was $p = 11.25$ mm, which is equivalent to a diffraction angle of $\alpha = 16^\circ$ in the first order according to the classic equation:

$$p \sin \alpha = m\lambda, \quad (1)$$

where $m = 1$ is the diffraction order and $\lambda = 3.1$ mm is the design wavelength. Such created object beam illuminates the first test transparency of a letter “E” (d). The secondary wavefronts emerging from (d) illuminate the second test transparency of a letter “C” (e) and then travel toward the detection plane, where the detector (f) is installed on a x - y - z scanning mount. The range of scanning is $400 \text{ mm} \times 300 \text{ mm}$ with a step of 1.25 mm in both directions. The test transparencies were 80-mm-tall capital letters cut out of an aluminum foil and partly covered with 5-mm-thick 3D-printed slabs of polylactic acid (PLA) for phase measurements, seen as darker parts of the letters. The reference beam formed by (c) travels at an angle of 16° and illuminates

the DOE#2 (g). The DOE#2 is a set of two sandwiched, fully modulated $p = 11.3$ mm sawtooth diffractive gratings, which diffract almost 100% of the reference beam toward the detection area at an angle of $2 \times 16^\circ = 32^\circ$. At the detection plane, the interference between two beams occurs and resultant interferometric fringes are recorded point by point in the x - y - z scanner carrying the LuviTera detector (f).

The crucial elements of the experimental setup are shown in Fig. 2. The DOEs (a) were designed in CAD software as first-order kinoforms [12, 13] and optimized numerically in an in-house wave optics software. The design was then exported to a STL file and printed in the SLS (selective laser sintering) technique in PA-12 material by a commercial entity to the final size of 360 mm \times 360 mm. The used LuviTera detector (b) was the dipole, log-periodic *THz_mini_wb* model, featuring the active antenna area of ~ 1.3 mm², the sensitivity of > 200 kV/W, and noise equivalent power (NEP) at < 20 pW/ $\sqrt{\text{Hz}}$. The mechanical x - y - z scanner was constructed with linear translation stages, controlled by the custom-programmed Arduino device via RS-232 protocol.

The exemplary captured interferogram consisting 160 \times 320 samples is shown in Fig. 3 (a). The high contrast of visible fringes proves that the optical path difference of the two THz beams was smaller than the coherence length of the used source. Moreover, it proves that the intensity and polarization of the two beams were undisturbed during the whole propagation [14]. The holographic reconstruction was performed by wave optics software (Ortech LightSword 6) utilizing the angular spectrum propagation method [15]. The matrix of real numbers was created by point-by-point importing of intensity values captured by the moving detector. Such interferogram then was propagated numerically to distances of 600 mm and 800 mm, respectively, and intensity fields were exported as seen in Fig. 3 (b, c). No pre-processing of the fringes was attempted proving the lack of stray fields in the detection plane. No postprocessing was done on the reconstructed intensity images, proving the high informative capacity of the recordings. The denser fringes of lower contrast, visible in the left-side part of the interferogram in Fig. 3, are the result of interference with higher orders of diffraction from the diffractive gratings, being the consequence of non-perfect 3D printing of grooves.

The hypothetical rotation of the polarization of any of the interfering beams would result in the partial loss of contrast of the fringes. Their contrast ratio was 49:1, as experimentally measured by dividing the maximal non-saturated intensity by the averaged background intensity. This value was affected by uncertainty due to sparse sampling; therefore, by repeating the measurement in different parts of the interferogram, the final value of $(48.6 \pm 0.7):1$ was obtained.

Figure 4 shows the cross-section of a few periods of the recorded fringes compared with theoretical cosine fringes of two beams with exactly parallel linear polarizations, simulated with Zemax OpticStudio in the same geometry, i.e., two plane waves interfering at an angle of 16° . The good fit allows to assume unitary contrast ratios obtained in our experiment, and in consequence, the indirect proof of maintained collinearity of polarizations of the interfering beams.

The polarization selectivity of the detector allowed us to examine the angle of polarization of all beams directly in the following experiment. The detector was placed in the central area of the intensity envelope of the examined beam and then rotated in full 180° range in 20° increments. After every rotation the intensity signal in a small area of 20 mm \times 30 mm was integrated and averaged. By

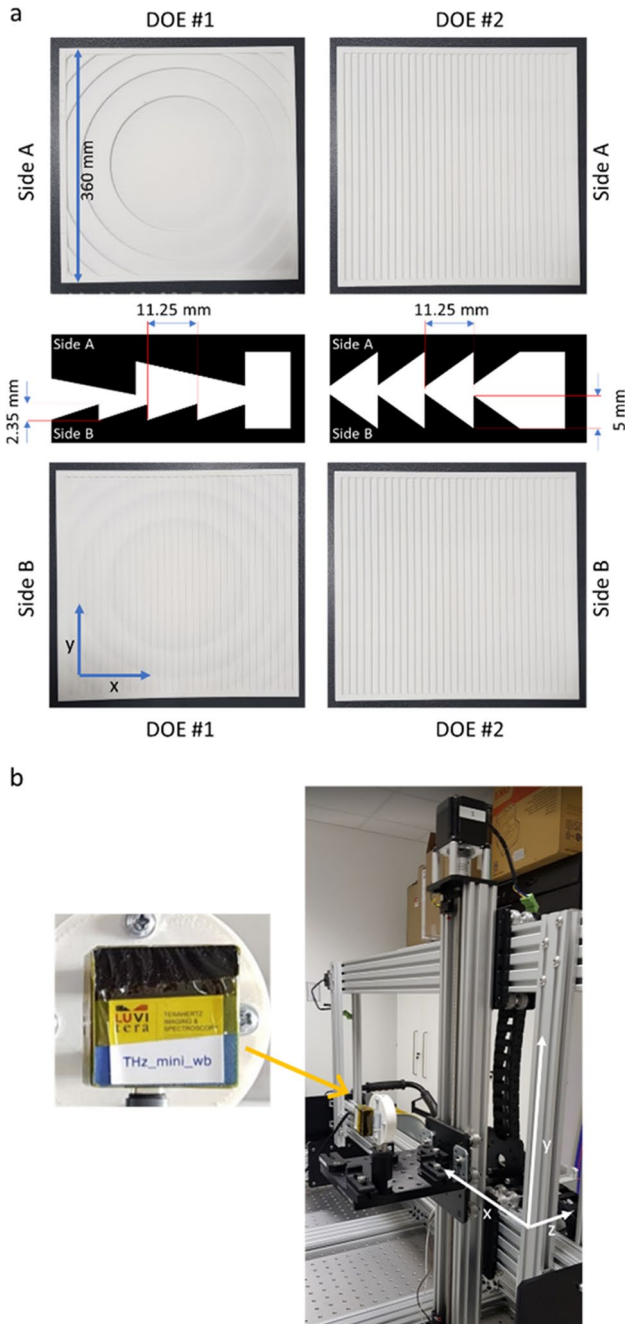


Fig. 2 Components of the experimental setup: **a** diffractive optical elements with halves of their cross-sections; **b** detector scanning system with a close-up of the detector on a rotating mount

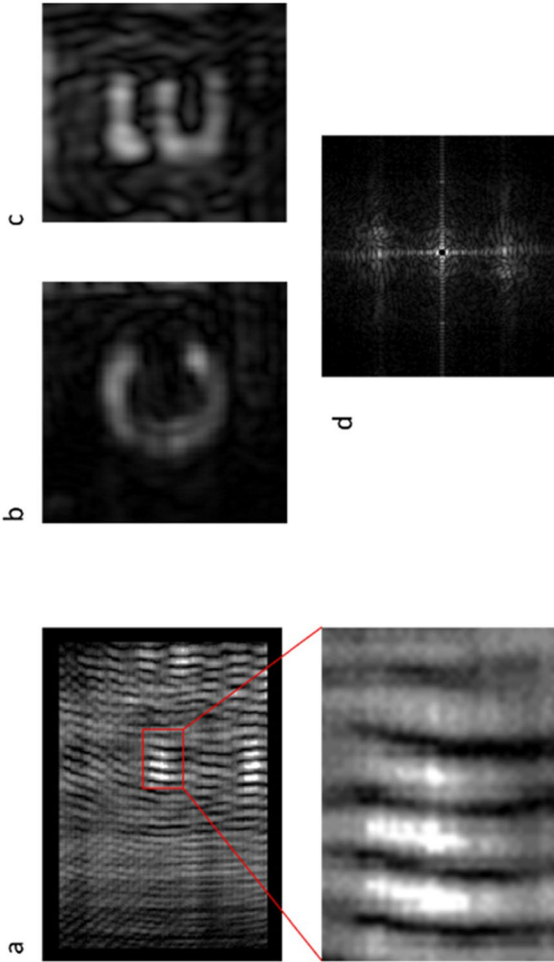


Fig. 3 **a** Exemplary raw interferogram captured in the experimental setup; unprocessed numerical reconstructions of the intensity of test transparencies at **b** 600 mm and **c** 800 mm; **d** frequency spectrum of the hologram

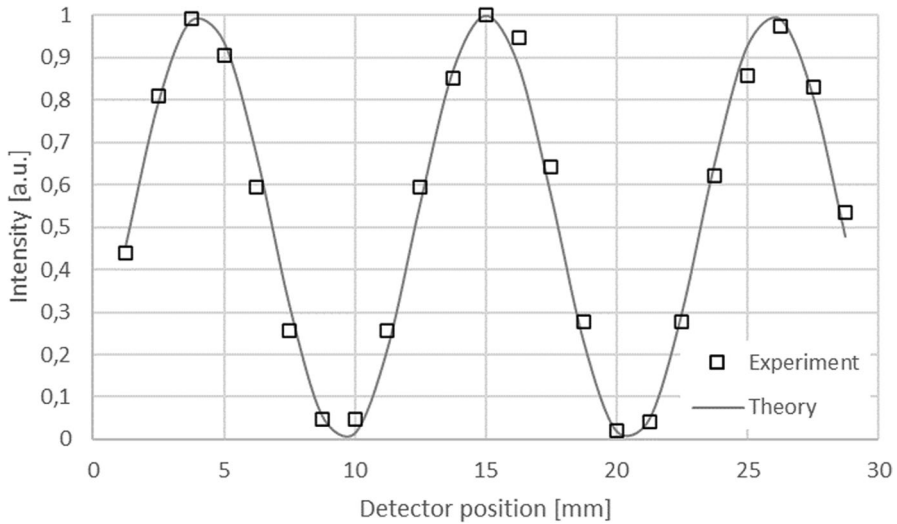


Fig. 4 Contrast of experimentally obtained interference fringes (squares) and theoretical fringes from two beams of colinear polarizations (solid line)

finding the global maximum in such created curves, as shown in Fig. 5, we were able to derive the angular orientation of the polarization of a tested beam.

Figure 5 compares the results for three beams: source beam (a), object beam (b), and the reference beam (c). The Gaussian fits clearly show the same positions of maxima, close to 0° . The visible noise was attributed to the presence of stray THz radiation from uncontrolled reflections, which could not be completely eliminated.

We have successfully demonstrated an alternative method of the off-axis digital holography with transmissive diffractive optical elements used to collimate and guide the terahertz beam. The elimination of mirrors facilitates setting up the experiment, as well as allows to reduce its cost and complexity, especially when the highly divergent THz beam is used, typically requiring large, off-axis parabolic mirrors. Moreover, any number and combination of proposed diffractive optical elements may be used without spurious rotations or alterations of the polarization of interfering beams, leading to superior contrast of fringes at the detection plane. The demonstration of more complex configurations is a matter of our future work.

The capability of 3D printing of DOEs in PA-12 [16] and other materials facilitates the prototyping and iterative optimization of the optical functionality with quick turnover and low costs. Low amounts of the dielectric material and large surface areas of the DOEs allow low signal attenuation in wide range of THz radiation, providing usefulness to a variety of experimental cases.

As an alternative to the recently reported shear interferometry [17], the proposed method allows the full utilization of the beam diameter.

Moreover, controllable modulation depth of DOEs allows an arbitrary division of the THz power into selected orders of diffraction, which opens the way to simplification of experimental methodology in terahertz interferometry with simple and demanding (i.e., reflective, absorbing) objects in numerous optical configurations.

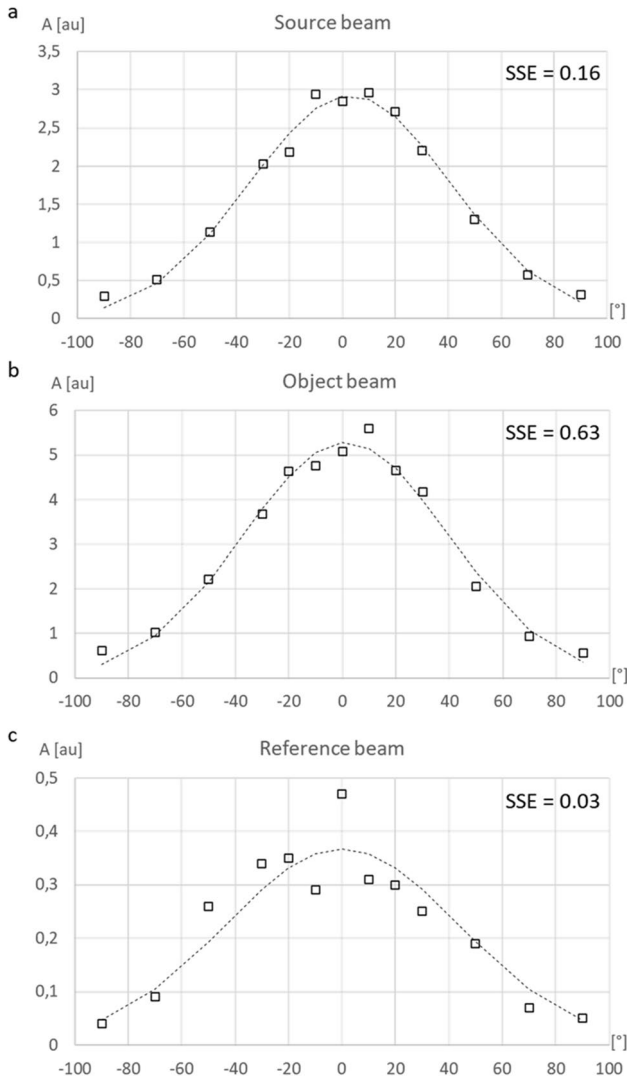


Fig. 5 Measurements of the polarization angles of THz beams: **a** source alone; **b** beam propagated through DOE#1; **c** beam propagated through DOE#2. Gaussian fittings are superimposed (dashed lines), showing the zero deviation. Sum of squared estimate of error (SSE) values are given as the estimation of the quality of fitting

Author Contributions A.S. conceived the idea and performed the experiment. M.M. wrote the main manuscript text and prepared the figures. A.K., J.S., and M.T. designed and constructed the experimental setup. M.S. did the literature research, secured the funding, and reviewed the manuscript.

Funding CB POB FOTECH-3 of Warsaw University of Technology; Excellence Initiative: Research University (IDUB) program.

Data Availability Data underlying the results presented in this paper are not publicly available at this time but may be obtained from the authors upon reasonable request.

Disclosures

Conflict of Interest The authors declare no competing interests.

Open Access This article is licensed under a Creative Commons Attribution 4.0 International License, which permits use, sharing, adaptation, distribution and reproduction in any medium or format, as long as you give appropriate credit to the original author(s) and the source, provide a link to the Creative Commons licence, and indicate if changes were made. The images or other third party material in this article are included in the article's Creative Commons licence, unless indicated otherwise in a credit line to the material. If material is not included in the article's Creative Commons licence and your intended use is not permitted by statutory regulation or exceeds the permitted use, you will need to obtain permission directly from the copyright holder. To view a copy of this licence, visit <http://creativecommons.org/licenses/by/4.0/>.

References

1. E. Cuche, P. Marquet, and C. Depeursinge, "Spatial filtering for zero-order and twin-image elimination in digital off-axis holography," *Appl. Opt.* **39**, 4070–4075 (2000).
2. Martin S. Heimbeck, and Henry O. Everitt, "Terahertz digital holographic imaging," *Adv. Opt. Photon.* **12**, 1–59 (2020).
3. M.S. Heimbeck, M.K. Kim, D.A. Gregory, and H.O. Everitt, "Terahertz digital holography using angular spectrum and dual wavelength reconstruction methods," *Opt. Express* **19**, 9192–9200 (2011).
4. Lee, A. W. M. et al., "Real-time terahertz imaging over a standoff distance (>25 m)," *Appl. Phys. Lett.* **89**, 141125 (2006).
5. M. Locatelli et al., "Real-time terahertz digital holography with a quantum cascade laser," *Sci. Rep.* **5**, 13566 (2015).
6. A.E. Shtanko et al., "Compensation of Aberrations of Off-Axis Parabolic Mirrors by Means of Digital Holography," *Meas. Tech.* **58**, 854–859 (2015).
7. U. Schnars, and W. Jüptner, "Digital Holography," Springer (2005).
8. E. Hack, and P. Zolliker, "Terahertz holography for imaging amplitude and phase objects," *Opt. Express* **22**, 16079–16086 (2014).
9. G.S. Kalenkov, S.G. Kalenkov, and A.E. Shtanko, "High aperture off-axis parabolic mirror applied in digital holographic microscopy," *Opt. Eng.* **57**, 043112 (2018).
10. M. Yokota, "Polarization analysis by off-axis digital holography with an improved optical system and an evaluation of its performance by simulation," *Appl. Opt.* **47**, 6325–6333 (2008).
11. A. Siemion, "Terahertz Diffractive Optics—Smart Control over Radiation," *J. Infrared. Milli. Terahz. Waves* **40**, 477–499 (2019).
12. J. Suszek, M. Sypek, M. Makowski, F. Garet, I. Ducin, K. Kakarenko, J. Bomba, and J.-L. Coutaz, "Evaluation of the shadow effect in terahertz kinoform gratings," *Opt. Lett.* **38**, 1464–1466 (2013).
13. J. Suszek et al., "High order kinoforms as a broadband achromatic diffractive optics for terahertz beams," *Opt. Express* **22**, 3137–3144 (2014).
14. J. Goodman, „Introduction to Fourier Optics," Roberts and Company Publishers; 3rd (2004).
15. M. Sypek, "Light propagation in the Fresnel region. New numerical approach," *Opt. Commun.* **116**, 43–48 (1995).
16. J. Bomba, J. Suszek, M. Makowski, A. Sobczyk, and M. Sypek, "3-D Printed Anti-Reflection Structures for the Terahertz Region," *J Infrared Milli Terahz Waves* **39**, 24–35 (2018).
17. M. Agour, C. Fallorf, F. Taleb, E. Castro-Camus, M. Koch, R.B. Bergmann, "Terahertz referenceless wavefront sensing by means of computational shear-interferometry," *Opt. Express* **30**, 7068–7081 (2022).

Publisher's Note Springer Nature remains neutral with regard to jurisdictional claims in published maps and institutional affiliations.